Effect of laminin, polylysine and cell medium components on the attachment of human hepatocellular carcinoma cells to cellulose nanofibrils analyzed by surface plasmon resonance

Zhang, Xue

2021-02-15

Zhang , X , Viitala , T , Harjumäki , R , Kartal-Hodzic , A , Valle-Delgado , J J & Österberg , M 2021 , ' Effect of laminin, polylysine and cell medium components on the attachment of human hepatocellular carcinoma cells to cellulose nanofibrils analyzed by surface plasmon resonance ' , Journal of Colloid and Interface Science , vol. 584 , pp. 310-319 . https://doi.org/10.1016/j.jcis.2020.09.

http://hdl.handle.net/10138/324199
https://doi.org/10.1016/j.jcis.2020.09.080

Journal of Colloid and Interface Science 584 (2021) 310–319

Contents lists available at ScienceDirect

Journal of Colloid and Interface Science

journal homepage: www.elsevier.com/locate/jcis

Regular Article

Effect of laminin, polylysine and cell medium components on the attachment of human hepatocellular carcinoma cells to cellulose nanofibrils analyzed by surface plasmon resonance

Xue Zhang [a], Tapani Viitala [b,1], Riina Harjumäki [a,b], Alma Kartal-Hodzic [b], Juan José Valle-Delgado [a,*], Monika Österberg [a,*]

[a] Department of Bioproducts and Biosystems, School of Chemical Engineering, Aalto University, FI-00076 Aalto, Finland
[b] Drug Research Program, Division of Pharmaceutical Biosciences, Faculty of Pharmacy, University of Helsinki, FI-00014 Helsinki, Finland

GRAPHICAL ABSTRACT

The adsorption of human hepatocellular carcinoma cells (HepG2) on cellulose nanofibril (CNF) films is studied in this work in real time by surface plasmon resonance. The effect of poly-L-lysine, laminin 521, and cell medium components on HepG2-CNF interaction is evaluated in order to develop future CNF-based systems with tuned cell adhesion properties for different tissue engineering applications. **Keyword:** Real time Cell Adhesion.

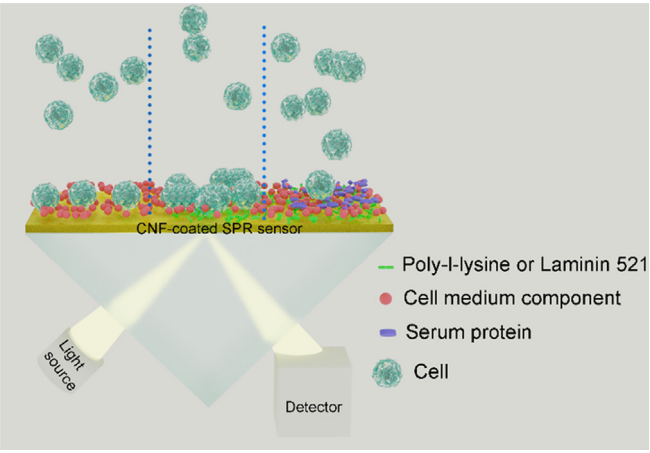

ARTICLE INFO

Article history:
Received 15 June 2020
Revised 22 August 2020
Accepted 20 September 2020
Available online 25 September 2020

Keywords:
Cellulose nanofibrils
Cell adsorption

ABSTRACT

The development of *in vitro* cell models that mimic cell behavior in organs and tissues is an approach that may have remarkable impact on drug testing and tissue engineering applications in the future. Plant-based, chemically unmodified cellulose nanofibrils (CNF) hydrogel is a natural, abundant, and biocompatible material that has attracted great attention for biomedical applications, in particular for three-dimensional cell cultures. However, the mechanisms of cell-CNF interactions and factors that affect these interactions are not yet fully understood. In this work, multi-parametric surface plasmon resonance (SPR) was used to study how the adsorption of human hepatocellular carcinoma (HepG2) cells on CNF films is affected by the different proteins and components of the cell medium. Both human recombinant laminin-

* Corresponding authors.
E-mail addresses: juanjose.valledelgado@aalto.fi (J.J. Valle-Delgado), monika.osterberg@aalto.fi (M. Österberg).
[1] Current address: Drug Research Program, Division of Pharmaceutical Chemistry and Technology, Faculty of Pharmacy, University of Helsinki, FI-00014 Helsinki, Finland.

https://doi.org/10.1016/j.jcis.2020.09.080
0021-9797/

Proteins
Surface plasmon resonance
Interactions

521 (LN-521, a natural protein of the extracellular matrix) and poly-L-lysine (PLL) adsorbed on CNF films and enhanced the attachment of HepG2 cells. Cell medium components (glucose and amino acids) and serum proteins (fetal bovine serum, FBS) also adsorbed on both bare CNF and on protein-coated CNF substrates. However, the adsorption of FBS hindered the attachment of HepG2 cells to LN-521- and PLL-coated CNF substrates, suggesting that serum proteins blocked the formation of laminin-integrin bonds and decreased favorable PLL-cell electrostatic interactions. This work sheds light on the effect of different factors on cell attachment to CNF, paving the way for the utilization and optimization of CNF-based materials for different tissue engineering applications.

1. Introduction

There is an increasing demand for accurate organ models for toxicology testing of drugs and chemicals and for organ replacements. Commonly used animal models for drug testing are both ethically questionable and not always accurate. Hence, the development of *in vitro* cell models that mimic the response of cells *in vivo* has attracted increasing attention lately [1]. Since the liver is the main organ responsible for drug metabolism and xenobiotic biotransformation, hepatic cell lines have been used in biomedical research for decades. Out of these, the human hepatocellular carcinoma cell line HepG2 has been a popular model for liver disease investigations, drug tests and genotoxicity studies [2]. HepG2 cells retain most of the main properties of normal liver parenchymal cells like, for instance, the biosynthesis of plasma proteins and the expression of many enzymes for xenobiotic biotransformation [3,4].

Three-dimensional (3D) cell cultures using natural biomaterials are promising alternatives for *in vitro* cell models that mimic *in vivo* cellular systems. Hydrogels of chemically unmodified, wood-derived cellulose nanofibrils (CNF, also called nanofibrillated cellulose, NFC) have been successfully used in 3D cell cultures [5–7]. CNF is a natural, abundant, low cost, and biocompatible material that has gained interest for biomedical applications due to its controllable viscoelastic properties. It has been reported that cells show low affinity for CNF [8]. The low affinity of cells for CNF could explain the suitability of CNF for the formation of cell spheroids, where cell-cell adhesion is more important than cell-material interactions, and for helping to maintain stem cells undifferentiated in 3D cell cultures [5,9]. Nevertheless, strong adhesion of cells to the scaffold may be required for other tissue engineering applications, such as constructing neural networks and bioartificial organs. Hence, proteins from extracellular matrix (ECM) are frequently used to enhance cell attachment to different substrates, such as bacterial nanocellulose [10], and to induce differentiation [11].

Laminin is a high-molecular weight (400–900 kDa), ECM glycoprotein composed of three chains –α, β, and γ chains– arranged in a four-arm extended structure [12]. Each chain contains distinct domains with different functions. In particular, the globular and rod-like domains promote the binding of laminin to cells and other ECM components [13,14]. The specific interaction of laminin with cell membrane receptors induces signals regulating cellular processes, such as cell adhesion, growth, proliferation and differentiation. Charonis et al. found that a heparin-binding domain of laminin promoted laminin adhesion to various cell lines [15]. Likewise, Timpl et al. demonstrated that rat hepatocyte adhesion was enhanced by several laminin fragments obtained by proteolysis [16]. However, natural ECM proteins are generally expensive and need low temperature storage. As an economic and easy option, the synthetic protein poly-L-lysine (PLL) has a long history in assisting cell cultivation, thanks to the favorable electrostatic interactions between its positively charged amine groups and the negatively charged cell surfaces. Thus, PLL has been used to assist cell attachment onto solid substrates for many purposes [17–22], including the analysis of the morphology and Young's modulus of living human B-lymphoma cells [18,19]. Due to the same electrostatic interaction, PLL could also be expected to enhance cell attachment to CNF surfaces. Although the adsorption of PLL on CNF has been studied before [23], the effect of PLL on cell adhesion to CNF has not been investigated to date.

Surface plasmon resonance (SPR) is a label-free, goniometer-based, surface sensitive and real-time monitoring technique that has become an interesting tool for live cell research. SPR measurements are based on the excitation of surface plasmons at the interface between a metal –usually gold– and a dielectric medium by plane-polarized light under total internal reflection conditions. The adsorption of a material on the metal surface affects the momentum of the plasmons, which can be monitored in real time by the shift in the angle of incidence of the light at which a minimum in reflectivity is observed [24,25]. SPR has been applied to monitor the real-time response of mast cells to reactive antigens [26], the response of NIH-3T3 fibroblast cells to trypsin, serum and sodium azide [27], the capture of nanoparticles by HeLa cells [28], and the coagulation of blood on different surfaces [29].

Cell culture media contain a plethora of electrolytes as well as sugars and amino acids to promote cell viability and growth. Co-factors like laminin and PLL are furthermore used to induce cell proliferation or cell adhesion. The affinity of cells to various cell culture materials have been discussed [30,31], and the effect of some serum proteins on cell adhesion has been inferred [32,33], but the role of cell medium components in cell-material interactions is largely unknown. In this study we used multi-parametric (two-wavelength) SPR [29,34,35] to systematically investigate the adsorption of the co-factors PLL and human recombinant laminin-521 (LN-521), and other cell medium components on CNF films. The thicknesses and refractive indices of the adsorbed layers were evaluated, but most importantly the effect of these cofactors on the adsorption of HepG2 cells on CNF was analyzed. The results of this work could facilitate the tailored design of CNF-based scaffolds for different cell culture and tissue engineering applications.

2. Experimental section

2.1. Materials

CNF hydrogel (Growdex®, UPM Corporation, Finland) with a nominal concentration of 15 g/L was used to prepare CNF dispersions. All the other chemicals were purchased from Sigma-Aldrich, Gibco, Riedel-de-Haën or VWR and used without any further purification. Further information about suppliers or product number can be found in the Methods section.

2.2. Methods

Preparation of CNF dispersions and PLL and LN-521 solutions: CNF dispersions were prepared according to the methods described by

Valle-Delgado et al. [36]. Briefly, CNF hydrogel was diluted in ultrapure water (Milli-Q, resistivity 18.2 MΩ·cm) and ultrasonicated for 1 min at 25% amplitude with a Branson sonifier S-450 D (Branson Corp., Danbury, CT). From the 1.9 g/L CNF dispersion obtained, larger aggregates were removed via centrifugation at 8000*g* for 30 min at room temperature with an Eppendorf centrifuge 5804R (Eppendorf, AG, Hamburg, Germany). Only the finest, well-dispersed fibrils from the supernatant were collected and utilized to prepare CNF films.

Aqueous 1 μg/mL PLL solutions were prepared by diluting 1 g/L PLL solution (Sigma-Aldrich) in ultrapure water.

LN-521 (LN521-02, BioLamina, Sundbyberg, Sweden) was diluted in Dulbecco's phosphate-buffer saline containing calcium and magnesium salts (DPBS+, Gibco™, from here on PBS+) according to the manufacturer's instructions to obtain a final concentration of 1 μg/mL.

Preparation of buffer solution: A buffer solution composed only of the inorganic salts in Dulbecco's Modified Eagle Medium (DMEM) cell medium –without amino acids, vitamins, glucose and other additives– was prepared. It contained 1.8 mM calcium chloride ($CaCl_2{\cdot}2H_2O$, ACS reagent (≥99%), Sigma-Aldrich), 2.48×10^{-4} mM ferric nitrate ($Fe(NO_3)_3{\cdot}9H_2O$, ACS reagent (≥98%), Sigma-Aldrich), 0.81 mM magnesium sulfate ($MgSO_4{\cdot}7H_2O$, ACS reagent (≥98%), Sigma-Aldrich), 5.3 mM potassium chloride (KCl, for analysis, EMSURE®, VWR), 44 mM sodium bicarbonate ($NaHCO_3$, analytical reagent (≥99.9%), Riedel-de-Haën), 110 mM sodium chloride (NaCl, ACS reagent (≥99.7%), Riedel-de-Haën, Sigma-Aldrich), and 0.92 mM sodium phosphate monobasic (NaH_2PO_4, reagent plus (≥99%), Sigma-Aldrich). The pH of the buffer was adjusted to 7.4 with hydrochloric acid (HCl, ACS reagent, 37%, Sigma-Aldrich).

Coating SPR sensors with CNF: CNF films were prepared by spin-coating CNF dispersions on gold SPR sensors (Bio Navis Ltd, Finland) using polyethyleneimine (PEI) as an adhesion promoter for CNF adsorption, as previously described by Valle-Delgado et al. [36] Briefly, SPR sensor surfaces were first cleaned in an ozone cleaner (UV.TC.EU.003, Ozonator, Bioforce Nanosciences. INC). Then, 200 μL 2.5 g/L PEI solution was dropped on the surface of each SPR sensor. PEI was allowed to adsorb for 10 min before rinsing with water. A few drops of the CNF dispersion were deposited on the PEI-coated SPR sensors and spin-coated at 4000 rpm for 1 min, with an acceleration of 2200 rpm/s using a Laurell spin-coater WS-650 SX-6NPP-Lite (Laurell Technologies Corp., North Wales, PA).

Cell maintenance: Human hepatocellular carcinoma HepG2 cells from ATCC (HB-8065) were cultured following the method described previously by Harjumäki et al. [8]. Briefly, HepG2 cells were seeded in 75 cm^2-cell culture flasks and maintained at 37 °C with 5% CO_2 incubator. The cell medium, CM (DMEM, Gibco, 41966-029) supplemented with 10% fetal bovine serum (FBS, Gibco, 10270-106) was used to culture HepG2 cells. TrypLE™ (GibcoTM, 12604-021) was used to passage cells twice a week at a ratio between 1:4 and 1:5 when the confluency reaches 70–90%.

Two-wavelength SPR measurements: Adsorption measurements on CNF-coated SPR sensors were performed with a multi-parametric SPR Navi 200 instrument (BioNavis Ltd, Tampere, Finland) in a Kretschmann configuration. The instrument provides two incident laser wavelengths, 670 nm and 785 nm. An electrochemical flow-cell (SPR 321-EC, BioNavis Ltd) with one flow channel was utilized. All the measurements were done in angular scan mode. The flow rate was 50 μL/min and the temperature was 37 °C for all set of experiments. Bare and CNF-coated gold SPR sensors were first measured in air for multilayer property analysis. Then, the CNF-coated SPR sensors were exposed to protein-free liquid media for 20 to 70 min to obtain stable baselines. The protein-free liquid media were the same media used to prepare PLL and LN-521 solutions, that is, ultrapure water and PBS+, respectively. In the following steps, PLL or LN-521 solutions, CM, and CM supplemented with 10% FBS were injected sequentially. The HepG2 adsorption experiments were conducted in both CM and CM supplemented with 10% FBS (FBS-CM) separately. Control experiments without PLL and LN-521 were also carried out.

All SPR data were processed by MP-SPR Navi Data viewer 4.3.3 software. A step by step optical characterization from the pure gold coated SPR sensor surface to a completed functionalized surface was accomplished in Layersolver 1.3.5 software (BioNavis Ltd,), using the two-wavelength data to determine layer thickness (d), refractive index (n) and imaginary part of refractive index (k) for each adsorbed layer. Taking into account that the adsorption of LN-521 and PLL may induce deswelling of the CNF layer, the fitting of LN-521 and PLL layers were performed while keeping the CNF layer parameters variable. In the fittings, n values were confined between 1.4 and 1.59, in accordance with literature values of refractive indices for cellulose and proteins [37,38]. Thickness and refractive index values are reported as mean values ± (maximum-minimum)/2 or mean values ± standard deviations for 2 or $2 < N \leq 6$ different experiments, respectively.

Atomic Force Microscopy (AFM): A MultiMode 8 atomic force microscope connected to a Nanoscope V controller (Bruker, Santa Barbara, CA) was used to provide high resolution images of CNF thin films. CNF-coated SPR sensors were imaged in tapping mode in air with an E scanner using NCHV-A probes (Bruker AFM probes, Camarillo, CA) to check the coverage of CNF fibrils on the sensors. CNF-coated SPR sensors after the adsorption of PLL and LN-521 during SPR experiments were also imaged in a similar manner. All the images were analyzed by NanoScope Analysis 1.5 software (Bruker). Flattening was the only applied correction.

Cell Viability Tests: Cell viability was tested on PLL and LN-521 coated coverslips (Sarstedt, 83.1840.002). 200 μL of 1 μg/mL PLL solution were dropped on top of each coverslip and adsorbed for 10 min. To remove any loosely attached PLL molecules, the PLL-coated coverslips were rinsed with ultrapure water and dried under nitrogen flow. The LN-521 coating was achieved by following the same procedure as described previously [39]. The coverslips were immersed in 1 μg/mL LN-521 solution and incubated for 2 h at room temperature. The LN-521 coated coverslips were then kept in PBS+ at +4 °C until cell seeding. Cells split from the same culture batch were seeded and maintained on PLL and LN-521 coated coverslips in FBS-CM for 20 h prior to testing cell viability. Trypan blue solution (0.4%, Gibco™ 15250-061) was dropped to cover the cell culture coverslips, and images were taken under Leica DM750 optical microscope (Leica Microsystems Schweiz AG).

3. Results and discussion

Despite its obvious advantage as a xeno-free and abundant material, CNF is still a rather novel cell culture material. Cell culturing systems are furthermore very complex, with many components and many interactions ongoing simultaneously. Understanding how cells interact with CNF and what factors affect these interactions is important for the development of optimal CNF-based culturing protocols and of CNF applications in tissue engineering. In the present study, SPR was used to investigate the interactions between HepG2 cells and CNF in a systematic way. More specifically, the effect of co-factors and cell medium components on these interactions was analyzed. A schematic illustration of the Krestschmann configuration of the SPR instrument used herein is shown in Fig. 1a. Fig. 1b shows a typical high-resolution AFM image of a CNF film spin-coated on an SPR sensor. CNF formed a fibrillar network that fully covered the gold surface of the SPR sensors. The CNF films were very smooth, with a root mean square (RMS) roughness of 4.4 ± 0.1 nm determined from

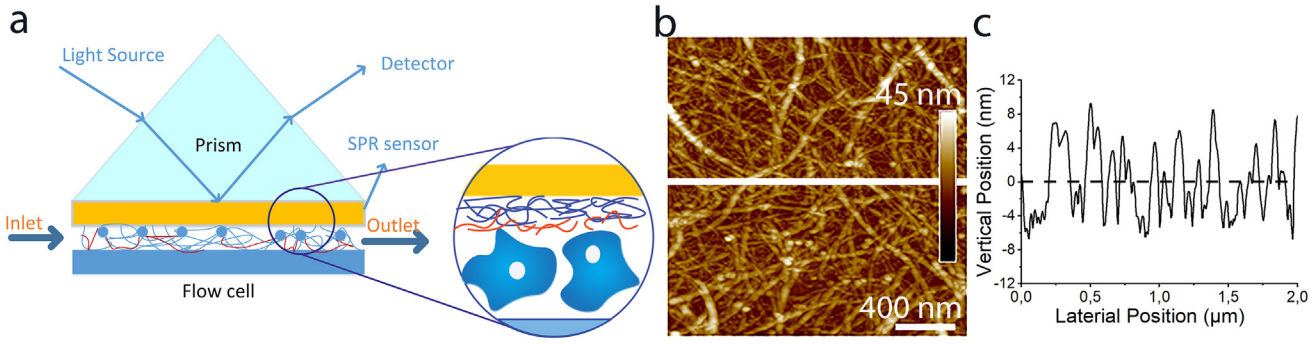

Fig. 1. Scheme of the SPR setup and characterization of a CNF-coated SPR sensor by AFM: (a) Kretschmann configuration of the SPR instrument, used for the cell adsorption experiments; (b) high-resolution AFM height image of a CNF film spin-coated on a SPR sensor; (c) cross-section profile corresponding to the white line in (b).

five 2 μm × 2 μm AFM images from different positions. The thickness of CNF films prepared by using the same protocol has been reported to be around 8 nm in the dry state [40,41], which was also the case in this study (Fig. 1c). The sequential adsorption of LN-521, PLL, CM, and FBS on CNF is presented in Section 3.1 (Figs. 2–4). The corresponding film thicknesses obtained from the fitting of the SPR data are summarized in Fig. 5. The adsorption of HepG2 cells on CNF films in the presence of different cofactors is shown and discussed in Section 3.2 (Figs. 6–8). SPR data at both 670 nm and 785 nm wavelengths were collected and analyzed to estimate the layer thicknesses. For the sake of clarity, only full SPR angular spectra at 785 nm are shown in the figures.

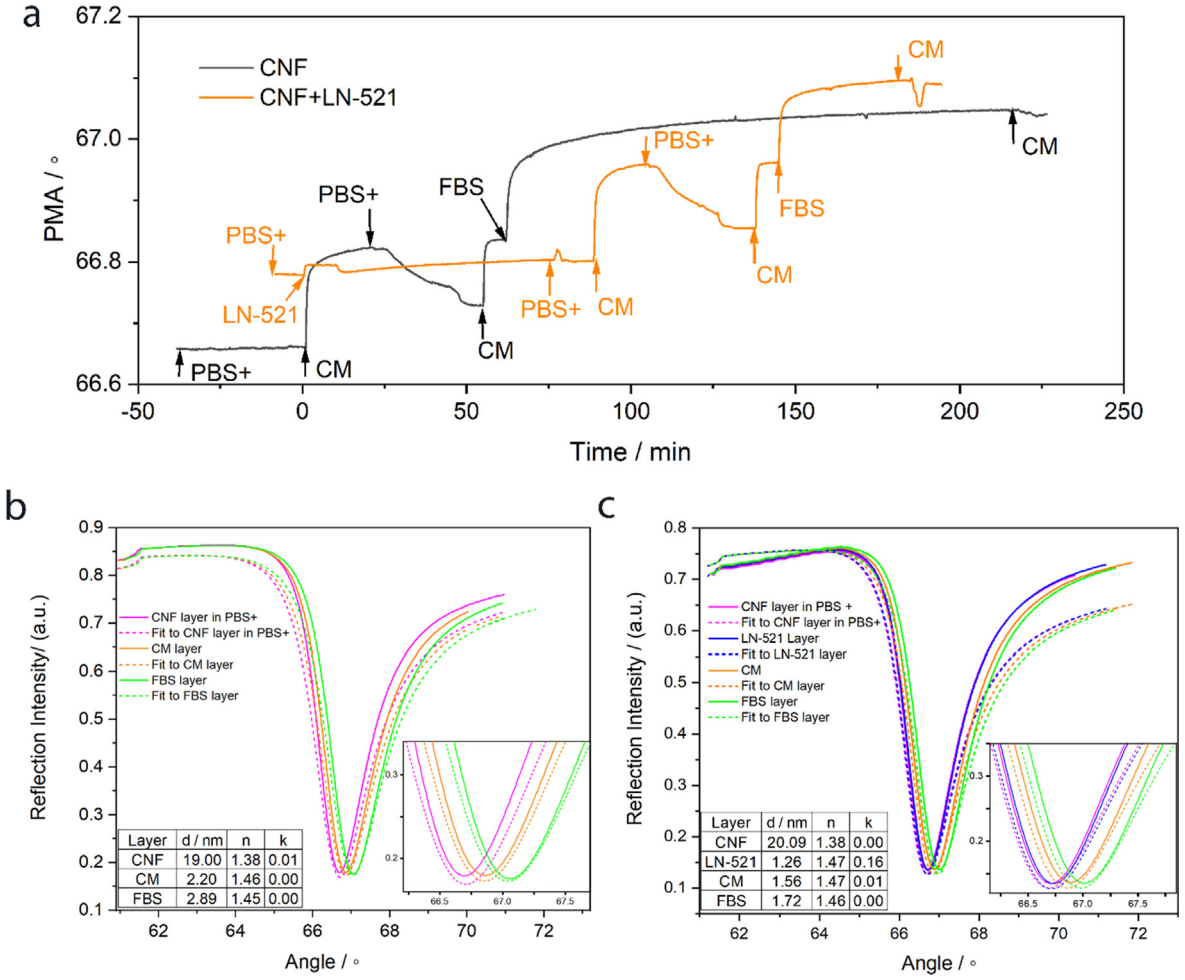

Fig. 2. Adsorption of LN-521, CM components and FBS on CNF-coated SPR sensors. (a) SPR sensogram showing the peak minimum angle (PMA) as a function of time during the sequential adsorption of LN-521, CM components and FBS (orange line). A control experiment without LN-521 is also shown (black line). The time for injecting LN-521 solution, FBS-free CM and FBS-containing CM are indicated with arrows (LN-521, CM, and FBS, respectively), as well as rinsing with PBS+. (b) SPR angular spectra and the corresponding fitting lines at time 0 min (CNF layer), 62 min (CM layer), and 225 min (FBS layer) for the adsorption experiment in the absence of LN-521 (black line in (a)). (c) SPR angular spectra and the corresponding fitting lines at time 0 min (CNF layer), 75 min (LN-521 layer), 138 min (CM layer) and 200 min (FBS layer) for the adsorption experiment in the presence of LN-521 (orange line in (a)).The fitting parameters *d*, *n*, and *k* shown in (b) and (c) correspond to one particular experiment. Average *d* values calculated from 3 to 6 independent experiments are plotted in Fig. 5. (For interpretation of the references to colour in this figure legend, the reader is referred to the web version of this article.)

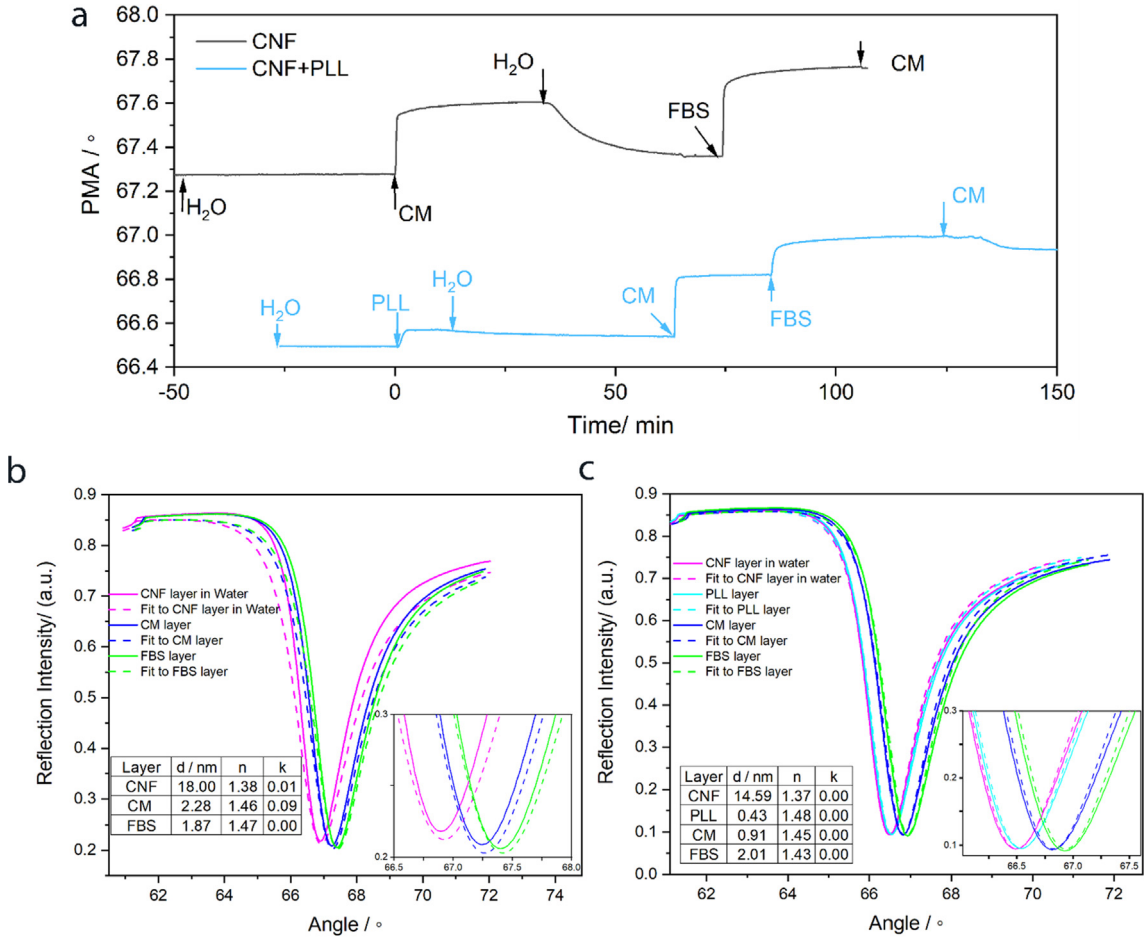

Fig. 3. Adsorption of PLL, CM components and FBS on CNF-coated SPR sensors. (a) Representative SPR sensogram showing the peak minimum angle (PMA) as a function of time during the sequential adsorption of PLL, CM components and FBS (blue line). A control experiment without PLL is also shown (black line). The time for injecting PLL solution, FBS-free CM and FBS-containing CM are indicated with arrows (PLL, CM, and FBS, respectively), as well as the rinsing with water. (b) SPR angular spectra and the corresponding fitting lines at time 0 min (CNF layer), 75 min (CM layer), and 108 min (FBS layer) for the adsorption experiment in the absence of PLL (black line in (a)). (c) SPR angular spectra and the corresponding fitting lines at time 0 min (CNF layer), 63 min (PLL layer), 83 min (CM layer) and 130 min (FBS layer) for the adsorption experiment in the presence of PLL (blue line in (a)).The fitting parameters *d, n*, and *k* shown in (b) and (c) correspond to one particular experiment. Average *d* values for 2 to 5 independent experiments are plotted in Fig. 5. (For interpretation of the references to colour in this figure legend, the reader is referred to the web version of this article.)

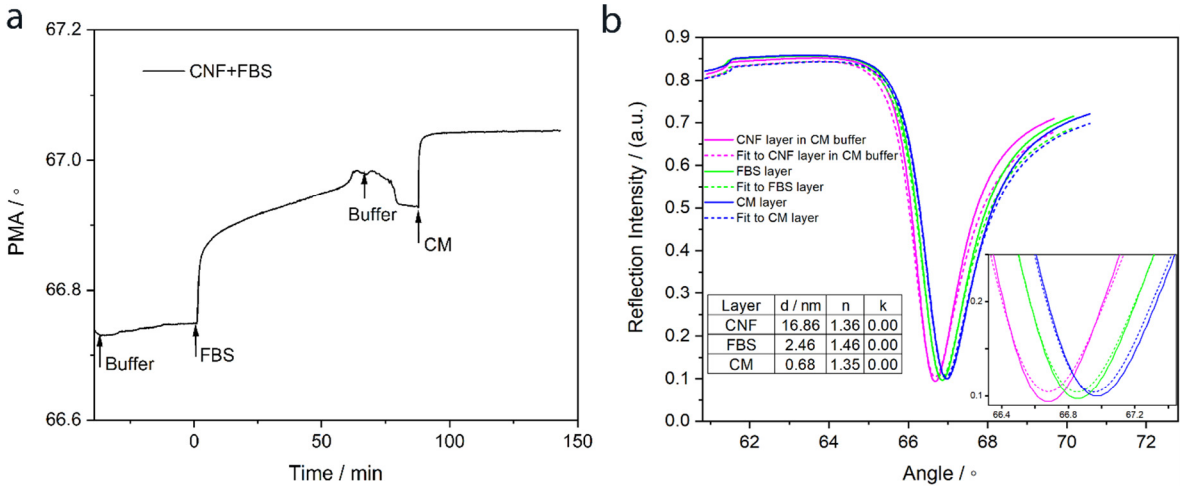

Fig. 4. Adsorption of FBS and CM components on CNF-coated SPR sensors. (a) SPR sensogram showing the peak minimum angle (PMA) as a function of time during the sequential adsorption of FBS and CM components. The time for injecting FBS-containing buffer and FBS-free CM are indicated with arrows (FBS and CM, respectively), as well as the rinsing with buffer. (b) SPR angular spectra and the corresponding fitting lines at time 0 min (CNF layer), 90 min (FBS layer), and 145 min (CM layer) for the adsorption experiment shown in (a). The fitting parameters *d, n*, and *k* shown in (b) correspond to one particular experiment. Averaged *d* values for 2 independent experiments are plotted in Fig. 5.

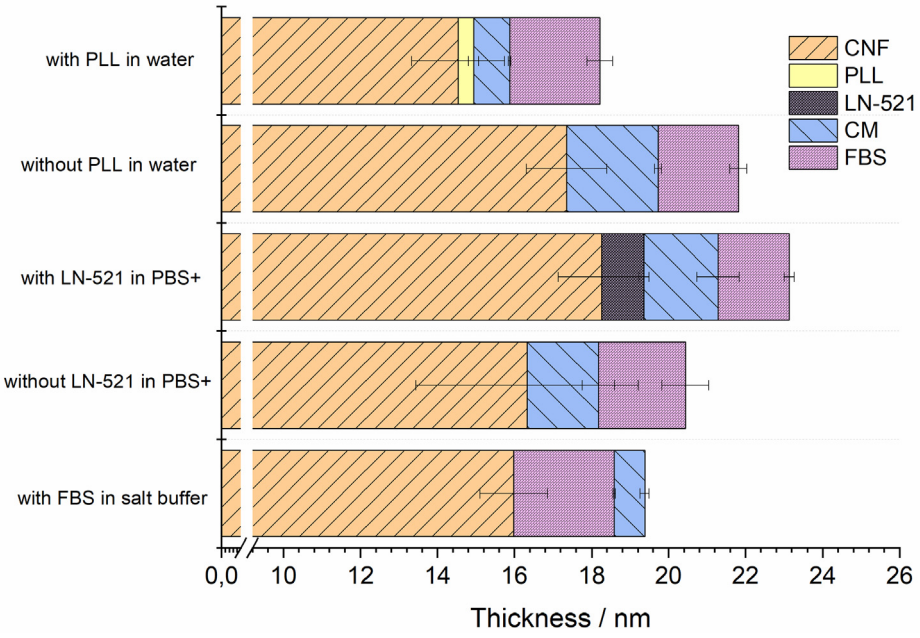

Fig. 5. Graphical summary of mean thickness values for the different material layers adsorbed on CNF films in different experiment types: Experiment type 1 (with PLL in water), sequential adsorption of PLL, CM components and FBS on CNF; Control 1 (without PLL in water), similar to Experiment type 1 but in the absence of PLL; Experiment type 2 (with LN-521 in PBS+), sequential adsorption of LN-521, CM components and FBS on CNF; Control 2 (without LN-521 in PBS+), similar to Experiment type 2 but in the absence of LN-521; Experiment type 3 (with FBS in salt buffer), sequential adsorption of FBS and CM components on CNF. The thickness values were obtained by fitting the corresponding SPR angular spectra layer after layer. CNF film thicknesses used when fitting the last adsorbed layer for each adsorption experiment are presented (swelling/deswelling of CNF films is shown in Fig. S2). Error bars correspond to standard deviation of 2 to 6 independent experiments. The specific number of experiments used for calculating the mean thickness values and the error bars are shown in Table S1. For all the experiment types, the sequential adsorption items are plotted from left to right.

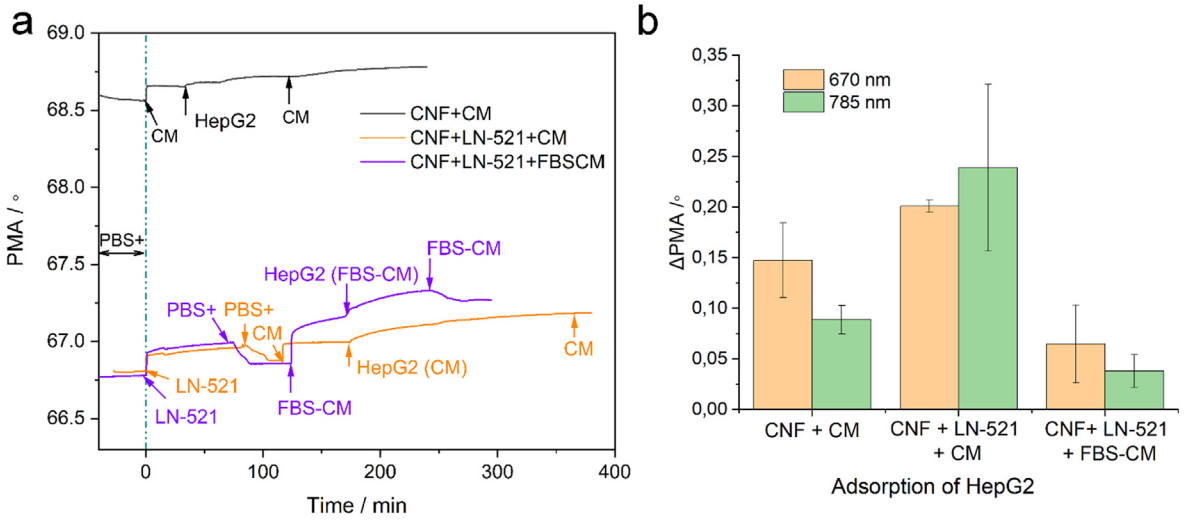

Fig. 6. The effect of LN-521 and FBS on HepG2 adsorption on CNF-coated SPR sensors. (a) SPR sensograms showing the peak minimum angle (PMA) as a function of time during the sequential adsorption of LN-521, CM components (with and without FBS) and HepG2 cells suspended in CM (with and without FBS, purple and orange lines, respectively). A control experiment without LN-521 and FBS is also shown (black line). The time for injecting LN-521 solution, CM (with and without FBS) and HepG2 cells suspended in CM (with and without FBS) are indicated with arrows (LN-521, CM or FBS-CM, and HepG2 (CM) or HepG2 (FBS-CM), respectively), as well as the rinsing with PBS+. (b) Change in PMA at 670 nm and at 785 nm wavelengths due to the adsorption of HepG2 cells on different CNF films with and without adsorbed LN-521 and FBS. Mean values and error bars of 2 independent experiments for each system are shown. (For interpretation of the references to colour in this figure legend, the reader is referred to the web version of this article.)

3.1. Adsorption of PLL, LN-521 and cell medium components on CNF

3.1.1. Adsorption of PLL and LN-521 on CNF

Cell adhesion, growth, and differentiation are highly dependent on cell adhesion proteins and extracellular components. Not all the cells are able to synthesize all these components, and, hence, proteins are frequently added to *in vitro* cultures to enhance cell proliferation or, in the case of stem cells, to induce differentiation [42]. Laminin, a cell secreted extracellular protein, is known to strongly adhere to hepatocytes [43]. PLL, an artificial synthesized protein, is widely applied either alone or as part of polyelectrolyte multilayers to enhance cell attachment on solid surfaces [22,44,45]. However, the co-function of these two types of proteins with the cell culture medium is still unknown.

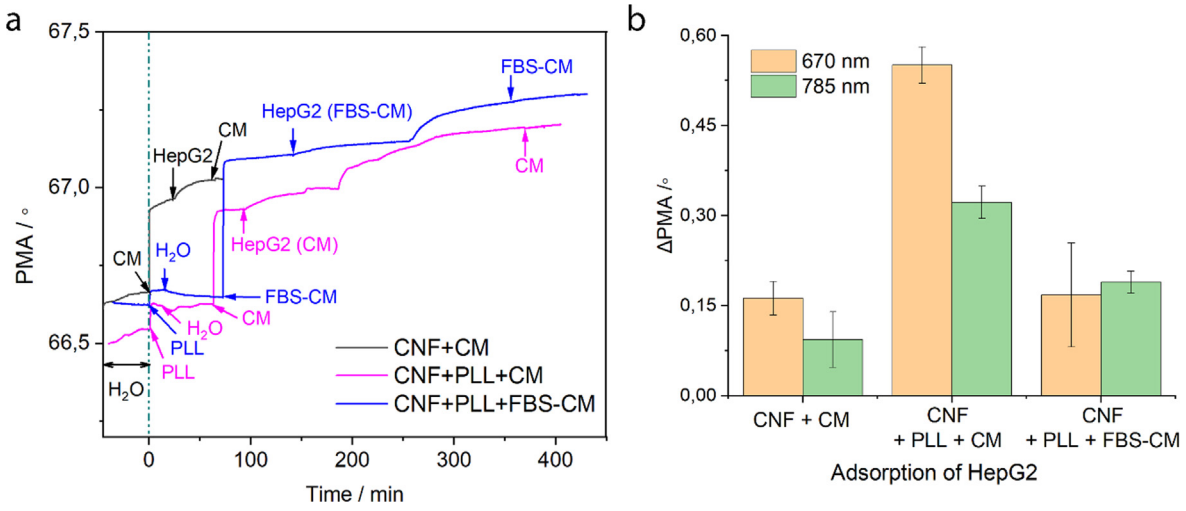

Fig. 7. The effect of PLL and FBS on HepG2 adsorption on CNF-coated SPR sensors. (a) SPR sensograms showing the peak minimum angle (PMA) as a function of time during the sequential adsorption of PLL, CM components (with and without FBS) and HepG2 cells suspended in CM (with and without FBS, blue and magenta lines, respectively). A control experiment without PLL and FBS is also shown (black line). The time for injecting PLL solution, CM (with and without FBS) and HepG2 cells suspended in CM (with and without FBS) are indicated with arrows (PLL, CM or FBS-CM, and HepG2 (CM) or HepG2 (FBS-CM), respectively), as well as the rinsing with water. (b) Change in PMA at 670 nm and at 785 nm wavelengths due to the adsorption of HepG2 cells on different CNF films with and without adsorbed PLL and FBS. Mean values and standard deviations (error bars) of 2 or 3 independent experiments are shown (N = 3 for CNF + CM system; N = 2 for CNF + PLL + CM and CNF + PLL + FBS-CM systems). (For interpretation of the references to colour in this figure legend, the reader is referred to the web version of this article.)

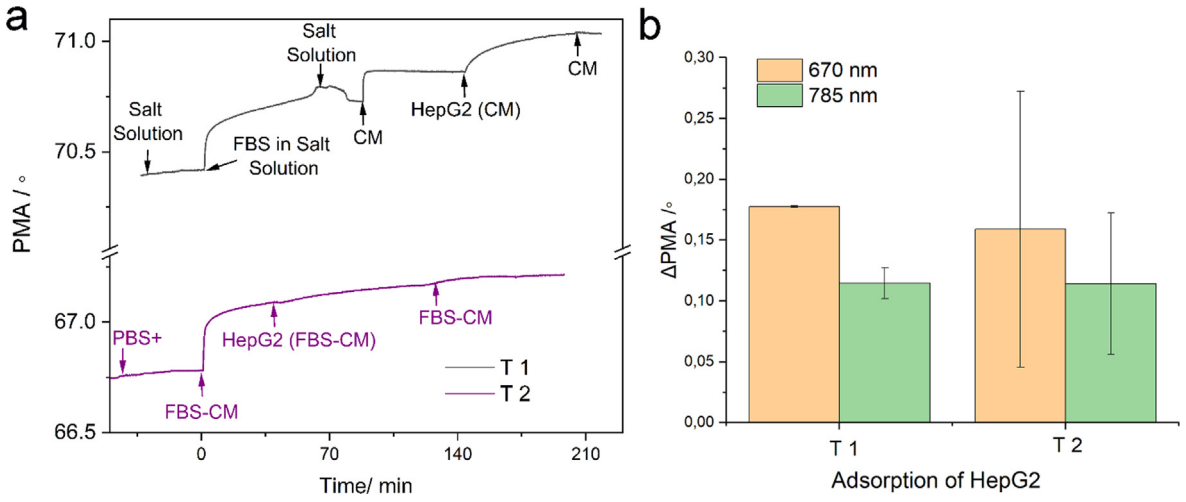

Fig. 8. HepG2 adsorption on CNF-coated SPR sensors in the presence of FBS. (a) SPR sensograms showing the peak minimum angle (PMA) as a function of time during the sequential adsorption of FBS and CM components (together or separately, purple and black lines, respectively) and HepG2 cells suspended in CM (with and without FBS, purple and black lines, respectively). The time for injecting FBS solution, CM (with and without FBS) and HepG2 cells suspended in CM (with and without FBS) are indicated with arrows (FBS, CM or FBS-CM, and HepG2 (CM) or HepG2 (FBS-CM), respectively), as well as the rinsing with buffer. (b) Change in PMA at 670 nm and at 785 nm wavelengths due to the adsorption of HepG2 cells on different CNF films with adsorbed FBS. Mean values and error bars of 2 independent experiments are shown. (For interpretation of the references to colour in this figure legend, the reader is referred to the web version of this article.)

The adsorption of LN-521 and PLL on CNF is shown in Figs. 2 and 3, respectively. Both LN-521 and PLL adsorbed onto CNF, forming thin layers that were not completely washed away when rinsing with PBS+ or ultrapure water, respectively. While some of the adsorbed LN-521 was removed upon rinsing, the adsorbed PLL layers were firmly attached and did not change upon rinsing. The adsorption trend of PLL on CNF shown in Fig. 3 is in line with previously published results by Forsman et al., who observed a rapid adsorption of PLL on CNF by the quartz crystal microbalance with dissipation monitoring (QCM-D) technique [23]. PLL is expected to interact with CNF mainly via electrostatic interactions between the positively charged, protonated amine groups of PLL and the slightly negatively charged CNF surfaces [40,46]. The adsorption of PLL on CNF could also be entropically favored by the release of bound water from the hydrated CNF films. Electrostatic interactions between oppositely charged groups is also a probable cause for the adsorption of LN-521 on CNF. The average layer thickness for LN-521 and PLL obtained by fitting the SPR data were 1.1 ± 0.2 n m and 0.4 ± 0.2 nm, respectively (Fig. 5). We speculate that the larger thickness values of the adsorbed LN-521 layer compared to PLL layer is due to the bulkier molecular structure of LN-521. Laminin is composed of three protein chains, whereas PLL is composed of only one molecular chain [12]. A looser conformation and thicker layer often leads to a weak adhesion. This may result in desorption of LN-521 upon rinsing. In agreement with the SPR results, no significant change in the morphology of the CNF films was observed in AFM images after the adsorption of LN-521 and PLL (Fig. S1), indicating that these proteins formed a very thin layer on CNF.

The interaction between CNF and different biomaterials has been quantified by AFM-colloidal probe microscopy previously

[39]. It was observed that the adhesion of CNF to LN-521 was significantly weaker than to type I and IV collagens. In spite of that, we observed here that the adhesion between CNF and LN-521 is strong enough for LN-521 to form a thin layer on top of CNF films that is not fully removed by rinsing (Fig. 2).

The CNF used here is a hydrophilic, slightly negatively charged natural material. The hydroxyl groups on the CNF surface can bind excess of water. In addition, water will be entrapped in the fibrillar network, resulting in highly swollen CNF gels or layers in aqueous media [35]. The extent of swelling depends on the ionic strength of the medium. Thus, CNF thicknesses of 21.9 ± 1.6 nm and 17.5 ± 2. 0 nm (Fig. S2) were obtained when equilibrating the CNF films in ultrapure water and PBS+, respectively (initial baselines in Figs. 2 and 3). It is interesting to note that the adsorption of PLL in water provoked a deswelling of the CNF layer, reducing the thickness to 16.3 ± 1.9 nm, similar as that in PBS+ with a higher ionic strength of 191 mM (Fig. S2). A similar deswelling upon adsorption of a highly cationic polyelectrolyte (PDADMAC) on CNF has been observed previously, due to the strong electrostatic interaction [47]. In contrast, the adsorption of LN-521 in PBS+ did not cause any further deswelling of CNF. In this case, the higher ionic strength of PBS+ was responsible of the CNF deswelling, which occurred before protein adsorption.

3.1.2. Effect of LN-521 on the adsorption of cell medium components on CNF films

Components in the cell medium (glucose, amino acids, vitamins, and serum) do not only supply the essential nutrients for cell proliferation but may also affect cell adhesion and interactions. Hence, the adsorption of cell medium components on CNF, and how LN-521 and PLL affect that adsorption, is relevant to understand cell behavior in CNF-based cell cultures.

Fig. 2 presents the adsorption of cell medium components on CNF films with and without adsorbed LN-521. Similar adsorption trends on CNF films were observed both in the presence and absence of LN-521. The adsorption sensograms in Fig. 2a show a change in the SPR peak minimum angle (PMA) after injecting the protein-free cell medium in the system, probably due to the adsorption of glucose, vitamins or amino acids from the cell medium. Rinsing with PBS+ partially removed the weakly adsorbed materials, which readsorbed after a new injection of cell medium. The subsequent introduction of FBS in the cell medium also provoked a clear change in PMA due to the adsorption of serum proteins [48–50].

Representative SPR angular spectra and the corresponding fitting lines are presented in Fig. 2b and c. The average of at least 4 independent experiments gave a thickness of 1.8 ± 0.4 nm and 1. 9 ± 0.6 nm for the adsorbed layer of cell medium components on CNF films both with and without LN-521 (Fig. 5). The average thicknesses obtained for the adsorbed FBS layers were 2.3 ± 0.6 n m and 1.9 ± 0.2 nm in the absence and presence of LN-521, respectively, which seems to indicate that LN-521 does not significantly affect the adsorption of serum proteins (Fig. 5).

It is worth noting that the change from PBS+ to cell medium and the adsorption of cell medium components did not affect the swelling of the CNF films, as both PBS+ and cell medium have high ionic strength. CNF film thicknesses of 17.5 ± 2.0 nm and 17.0 ± 2.6 nm were obtained in PBS+ and cell medium, respectively (Fig. S2).

3.1.3. Effect of PLL on the adsorption of cell medium components on CNF films

The effect of PLL on the adsorption of cell medium components on CNF films was studied as above with LN-521 (Fig. 3). The representative adsorption sensograms are presented in Fig. 3a. The injection of protein-free cell medium provoked a quick shift of the PMA towards higher angles both in the absence and presence of PLL. As mentioned above, vitamins, glucose, and amino acids from protein-free cell medium tend to adsorb on CNF film rapidly following injection. These compounds also adsorbed when PLL was present on the CNF surface, probably via electrostatic or van der Waals interactions with PLL. In addition, it is interesting to observe that the adsorbed material could be completely removed by rinsing with ultrapure water (Fig. S3) when PLL was present but was only partially removed in the absence of PLL (Fig. S3). This suggests that the binding of cell medium components to PLL is weaker than to CNF in water. It may indicate that glucose from CM shows a stronger interaction to the glucose units in CNF than to PLL. A similar adsorption of negatively charged or neutral polysaccharides onto CNF not through electrostatic interactions has been reported for negatively charged carboxymethylated cellulose and xylan, and for neutral xyloglucan and guar gum [40,51,52]. In any case, readsorption of cell medium components on CNF films with and without PLL was observed after re-injecting cell medium (Fig. S3).

An additional shift in PMA was observed after injecting the FBS-containing cell medium, revealing a fast adsorption of serum proteins. This layer was not greatly affected by the following rinse with FBS-free cell medium. Representative SPR angular spectra and the corresponding fitting lines are shown in Fig. 3b and c. PLL significantly reduced the adsorption of cell medium components on CNF films, as observed from the decrease in the thickness of the CM layer in the presence of PLL (Fig. 3b and c). The average thickness of adsorbed CM layers decreased from 2.4 ± 0.1 nm in the absence of PLL to 0.9 ± 0.1 nm in the presence of PLL (Fig. 5). In contrast, no significant difference was observed between the average FBS layer thickness in the absence or the presence of PLL (2.1 ± 0. 2 nm and 2.3 ± 0.3 nm, respectively), suggesting that PLL does not significantly affect the adsorption of serum proteins like bovine serum albumin.

As an additional observation, the adsorption of PLL provoked a deswelling of the CNF films, reducing their thicknesses from 21.9 ± 1.6 nm to 16.3 ± 1.9 nm in water, as noted before. Changing the ionic strength of the medium by the injection of cell medium caused an additional deswelling of the CNF films, shrinking to 14. 5 ± 1.2 nm (Fig. S2).

3.1.4. Adsorption of pure FBS on CNF films

The cell medium is a mixture of components and it is difficult to know what component is adsorbing on the CNF. To better understand the competition between FBS and other CM components for binding to CNF, FBS-containing buffer was prepared with the same composition of inorganic salts as the CM, but with none of the other compounds that may compete for adsorption sites with FBS. Adsorption experiments were carried out by injecting the FBS electrolyte buffer in the SPR chamber before injecting FBS-free CM (Fig. 4). The SPR sensograms show that both FBS and CM components adsorbed on CNF in this experimental configuration (Fig. 4a). The fitting of the angular spectra revealed that the thickness of the adsorbed FBS layer was barely affected by the order of injection of FBS and CM. The thickness was 2.6 ± 0.1 nm when FBS was injected before CM, however, when FBS was injected after CM (in the experiments without LN-521 and without PLL) the thickness of FBS layers were 2.3 ± 0.6 nm and 2.1 ± 0.2 nm, respectively (Fig. 5). In addition, compared to the thickness of the adsorbed CM components in the experiments without LN-521 (1.9 ± 0.4 nm) and without PLL (2.4 ± 0.1 nm), injecting CM after FBS significantly reduced the thickness of the adsorbed layer of CM components (0.8 ± 0.1 nm) (Figs. 4b and 5). Therefore, these results indicate that the adsorption of FBS on CNF was just slightly affected by the presence of other CM components. In contrast, the adsorption of CM components like glucose, vitamins or amino acids on CNF was significantly hindered in the presence of FBS.

3.2. Adsorption of HepG2 cells on CNF films

HepG2 cells have been observed to attach and grow on LN-521 [8]. In addition, PLL with grafted arabinogalactan has been used as a specific DNA carrier for HepG2 [53], but the interaction between PLL and HepG2 has not been studied so far. Furthermore, the effect of LN-521 and PLL on the interactions between HepG2 cells and CNF is still unclear. Hence, SPR experiments were carried out in this work to shed light on the effect of LN-521, PLL, and different factors in the cell culture medium on HepG2 attachment to CNF films. It should be borne in mind that SPR provides information about material adsorption only within a few hundreds of nanometers from the gold surface of the sensors, that is, the penetration depth of the evanescent wave of the plasmons. However, HepG2 cells are several micrometers in size. Thus, HepG2 adsorption was evaluated from the change in PMA, and no data fitting to obtain thickness values was attempted. For comparison, the cells were also seeded on glass substrates coated with PLL or LN-521. Compared to LN-521, HepG2 demonstrated a higher confluence on PLL-coated glass substrates after 20 h incubation (Fig. S4).

3.2.1. Effect of LN-521 on HepG2 adsorption on CNF films

Fig. 6 shows the effect of LN-521 and FBS on the adsorption of HepG2 on CNF films. The SPR sensograms in Fig. 6a present the entire experimental sequence: after the initial equilibration of CNF films in PBS+, a LN-521 solution was injected in the SPR chamber followed by either CM or FBS-containing CM, just before introducing the HepG2 cells (suspended in CM or FBS-containing CM, respectively), finally, either CM or FBS-containing CM were introduced to rinse the loosely adsorbed HepG2 cells. It should be noted that the cells were introduced to the SPR chamber using the same cell medium injected in the previous step, and only after a stable PMA value was obtained –indicating saturation of the adsorption of cell medium components. In this way, the change in PMA observed after the introduction of the cells could be confidently ascribed to HepG2 adsorption, and not to the adsorption of components from the cell medium. A control experiment for the adsorption of HepG2 cells in the absence of both LN-521 and FBS is also shown in Fig. 6a. The changes in PMA indicate that LN-521 adsorbed onto CNF but it was partially detached during rinsing with PBS+. CM components and FBS also adsorbed as was previously observed in Fig. 2. It can also be noted in Fig. 6a that the initial adsorption of HepG2 cells on LN-521-coated CNF appears similar both in CM and FBS-CM, but some cells detach during rinsing only when FBS was injected in the system before the HepG2 cells. The net changes in PMA due to the adsorption of HepG2 cells –after rinsing with the corresponding medium– are shown in Fig. 6b. In the absence of FBS, HepG2 adsorption on CNF films was enhanced by the presence of LN-521. Laminin is a ligand of HepG2 cell-membrane receptors called integrins [54]. Therefore, specific laminin-integrin interactions may be responsible for the enhanced adsorption of HepG2 cells on CNF films coated with LN-521. On the other hand, the adsorption of FBS from cell medium decreased the HepG2 adsorption, suggesting that FBS blocks laminin-integrin binding and, consequently, hinders HepG2 attachment to CNF films modified with LN-521.

The big error bars in Fig. 6b can be due to variability in cell activity in different cell passages (cell activities usually decreased as the number of passages increased). Regardless of the rather large variability, the trend was reproducible.

3.2.2. Effect of PLL on HepG2 adsorption on CNF films

The effect of PLL on the adsorption of HepG2 on CNF films in the presence and absence of FBS is shown in Fig. 7. The sequential adsorption of PLL, components of CM with or without supplemental FBS, and HepG2 cells, as well as a control experiment without PLL and FBS, are presented in Fig. 7a. The changes in PMA detected after the injection of HepG2 cells (suspended in either CM or FBS-containing CM) indicated cell adsorption. No cell detachment was seen during the final rinsing with the corresponding cell medium (Fig. 7a). It was observed that, in the absence of FBS, PLL enhanced HepG2 adsorption on CNF films; that is probably due to favorable electrostatic interactions between positively charged PLL and negatively charged cell membranes. However, the presence of FBS cancelled the effect of PLL, yielding PMA values for HepG2 adsorption similar or only slightly higher than the ones obtained in control experiments without PLL. Thus, the adsorption of serum proteins (mainly bovine serum albumin, BSA) on PLL-coated CNF films hindered, but did not completely block, the adhesion of HepG2 cells. BSA has been extensively used in biological applications such as immunoassays and targeted biomedical imaging due to its capability of reducing nonspecific interactions [55,56]. The decrease in HepG2 adsorption observed in Fig. 7b might also be due to the antifouling property of BSA, since it can reduce the non-specific cell-PLL attractive interactions and, correspondingly, HepG2 adhesion.

3.2.3. Effect of FBS on HepG2 adsorption on CNF films

The adsorption of FBS on both LN-521 and PLL-coated CNF films hindered the attachment of HepG2 cells as shown in Figs. 6 and 7. To further understand the role of the serum proteins on cell attachment, HepG2 cell adsorption on FBS-coated CNF films was investigated (Fig. 8). In these experiments FBS was first adsorbed on CNF directly, either from the cell medium or from the buffer solution with similar composition of inorganic salts. In both cases, an increase in PMA was observed in the sensograms after injecting the cells (Fig. 8a). The increase in PMA was of similar magnitude in both approaches (Fig. 8b), showing no effect of the way how FBS was adsorbed on CNF, that is, HepG2 showed similar adsorption when FBS was first adsorbed alone or together with other cell medium components. Curiously, the increase in PMA was also quite similar to the values obtained for the cell adsorption on CNF in FBS-free control experiments (Figs. 6b and 7b). These results suggest that the affinity of HepG2 cells for FBS is like the one for CNF, but clearly lower than for LN-521 or PLL. It has been found earlier that the interactions between CNF and HepG2 are weak and mainly nonspecific [57]. FBS contains mainly BSA, which is rich in carboxyl and amine groups, hormones and growth factors etc. [58]. The attractive interaction between HepG2 and FBS components also seems to be weak and probably nonspecific. In contrast, the specific binding of LN-521 to integrin on HepG2 membrane and the stronger electrostatic attraction between PLL and HepG2 considerably enhance HepG2 adsorption.

4. Conclusions

The chemically unmodified, wood-derived cellulose nanofibril hydrogel (CNF) is a natural, abundant, and biocompatible material that has emerged in the last years as a promising matrix for three-dimensional (3D) cell cultures [6,7]. The use of CNF to its full potential in tissue engineering and other biomedical applications requires a deep understanding of the cell-CNF interactions, as well as how different factors, like proteins and cell medium components, may affect those interactions. In this work, we present, for the first time, a systematic analysis of the real-time adsorption of a model cell line (human hepatocellular carcinoma, HepG2 cells) on CNF substrates using multi-parametric surface plasmon resonance (SPR), a label-free and surface sensitive technique. The modulation of the cell affinity for CNF by poly-L-lysine (PLL), laminin 521 (LN-521), serum proteins, and other cell medium components was also demonstrated. The attachment of HepG2 cells to CNF was

significantly enhanced after adsorbing PLL and LN-521 on CNF, demonstrating a way of increasing cell-CNF affinity. Cell medium components (glucose, amino acids, vitamins) and fetal bovine serum (FBS) proteins were also observed to adsorb on CNF films, both in the presence and absence of LN-521 and PLL. The adsorption of FBS, in particular, hindered HepG2 adsorption on CNF films coated with LN-521 and PLL, suggesting that FBS blocks specific laminin-integrin binding and diminishes favorable PLL-cell electrostatic interactions. The 2D adsorption results obtained in this work may be directly translated to 3D CNF-based scaffolds for different biomedical applications. The cell binding affinity of CNF-based scaffolds fabricated by 3D printing techniques can be enhanced by adsorbing PLL or LN-521, and by controlling the amount of serum proteins in the cell medium. This work also confirms the potential of surface plasmon resonance to study cell adsorption in real time.

CRediT authorship contribution statement

Xue Zhang: Methodology, Investigation, Visualization, Writing - original draft, Formal analysis. **Tapani Viitala:** Conceptualization, Methodology, Resources, Writing - review & editing. **Riina Harjumäki:** Methodology, Writing - review & editing. **Alma Kartal-Hodzic:** Methodology. **Juan José Valle-Delgado:** Writing - review & editing, Supervision. **Monika Österberg:** Conceptualization, Writing - review & editing, Supervision, Funding acquisition.

Declaration of Competing Interest

The authors declare that they have no known competing financial interests or personal relationships that could have appeared to influence the work reported in this paper.

Acknowledgements

The authors thank the Academy of Finland for the financial support for this work (Project Number 278279, MIMEGEL), and Mauri Kostiainen and his group for the use of cell culture facilities at Aalto University. Xue Zhang thanks Dr. Apeksha Damania for helping with cell cultures. Xue Zhang is grateful for the financial support from both the FinnCERES Materials Bioeconomy Ecosystem and Puunjalostusinsinöörit ry, PI while preparing the manuscript. This work made use of Aalto University Bioeconomy Facilities.

Appendix A. Supplementary material

Supplementary data to this article can be found online at https://doi.org/10.1016/j.jcis.2020.09.080.

References

[1] M. Ravi, V. Paramesh, S.R. Kaviya, E. Anuradha, F.D.P. Solomon, J. Cell. Physiol. 230 (2015) 16.
[2] V. Mersch-Sundermann, S. Knasmüller, X.J. Wu, F. Darroudi, F. Kassie, Toxicology 198 (2004) 329.
[3] B.B. Knowles, C.C. Howe, D.P. Aden, Science 209 (1980) 497.
[4] D.P. Aden, A. Fogel, S. Plotkin, I. Damjanov, B.B. Knowles, Nature 282 (1979) 615.
[5] Y.R. Lou, L. Kanninen, T. Kuisma, J. Niklander, L.A. Noon, D. Burks, A. Urtti, M. Yliperttula, Stem Cells Dev. 23 (2014) 380.
[6] M. Bhattacharya, M.M. Malinen, P. Lauren, Y.R. Lou, S.W. Kuisma, L. Kanninen, M. Lille, A. Corlu, C. Guguen-Guillouzo, O. Ikkala, A. Laukkanen, A. Urtti, M. Yliperttula, J. Control. Release 164 (2012) 291.
[7] R. Ajdary, S. Huan, N.Z. Ezazi, W. Xiang, R. Grande, H.A. Santos, O.J. Rojas, Biomacromolecules 20 (2019) 2770.
[8] R. Harjumäki, R.W.N. Nugroho, X. Zhang, Y.R. Lou, M. Yliperttula, J.J. Valle-Delgado, M. Österberg, Sci. Rep. 9 (2019) 7354.
[9] M.M. Malinen, L.K. Kanninen, A. Corlu, H.M. Isoniemi, Y.R. Lou, M.L. Yliperttula, A.O. Urtti, Biomaterials 35 (2014) 5110.
[10] V. Kuzmenko, S. Sämfors, D. Hägg, P. Gatenholm, Mater. Sci. Eng. C 33 (2013) 4599.
[11] Y. Zhang, Y. He, S. Bharadwaj, N. Hammam, K. Carnagey, R. Myers, A. Atala, M. Van Dyke, Biomaterials 30 (2009) 4021.
[12] Y.C. Gu, J. Kortesmaa, K. Tryggvason, J. Persson, P. Ekblom, S.E. Jacobsen, M. Ekblom, Blood 101 (2003) 877.
[13] P.D. Yurchenco, Y.S. Cheng, H. Colognato, J. Cell Biol. 117 (1992) 1119.
[14] R. Timpl, H. Rohde, P.G. Robey, S.I. Rennard, J.M. Foidart, G.R. Martin, J. Biol. Chem. 254 (1979) 9933.
[15] A.S. Charonis, A.P.N. Skubitz, G.G. Koliakos, L.A. Reger, J. Dege, A.M. Vogel, R. Wohlhueter, L.T. Furcht, J. Cell Biol. 107 (1988) 1253.
[16] R. Timpl, S. Johansson, V. van Delden, I. Oberbäumer, M. Höök, J. Biol. Chem. 258 (1983) 8922.
[17] V. Ierardi, A. Niccolini, M. Alderighi, A. Gazzano, F. Martelli, R. Solaro, Microsc. Res. Tech. 71 (2008) 529.
[18] M. Li, L. Liu, N. Xi, Y. Wang, Z. Dong, O. Tabata, X. Xiao, W. Zhang, Biochem. Biophys. Res. Commun. 404 (2011) 689.
[19] M. Li, L.Q. Liu, N. Xi, Y.C. Wang, Z.L. Dong, X.B. Xiao, W.J. Zhang, Sci. China Life Sci. 56 (2013) 811.
[20] D. Mazia, G. Schatten, W. Sale, J. Cell Biol. 66 (1975) 198.
[21] V.D. Vacquier, Dev. Biol. 43 (1975) 62.
[22] G.E. Fantner, R.J. Barbero, D.S. Gray, A.M. Belcher, Nat. Nanotechnol. 5 (2010) 280.
[23] N. Forsman, A. Lozhechnikova, A. Khakalo, L.S. Johansson, J. Vartiainen, M. Österberg, Carbohydr. Polym. 173 (2017) 392.
[24] R.J. Green, R.A. Frazier, K.M. Shakesheff, M.C. Davies, C.J. Roberts, S.J.B. Tendler, Biomaterials 21 (2000) 1823.
[25] S. Lieb, S. Michaelis, N. Plank, G. Bernhardt, A. Buschauer, J. Wegener, Pharmacol. Res. 108 (2016) 65.
[26] M. Hide, T. Tsutsui, H. Sato, T. Nishimura, K. Morimoto, S. Yamamoto, K. Yoshizato, Anal. Biochem. 302 (2002) 28.
[27] Y. Shevchenko, G. Camci-Unal, D.F. Cuttica, M.R. Dokmeci, J. Albert, A. Khademhosseini, Biosens. Bioelectron. 56 (2014) 359.
[28] T. Suutari, T. Silen, D. Şen Karaman, H. Saari, D. Desai, E. Kerkelä, S. Laitinen, M. Hanzlikova, J.M. Rosenholm, M. Yliperttula, T. Viitala, Small 12 (2016) 6289.
[29] K.M. Hansson, P. Tengvall, I. Lundström, M. Rånby, T.L. Lindahl, Biosens. Bioelectron. 17 (2002) 747.
[30] A.J. García, P. Ducheyne, D. Boettiger, Biomaterials 18 (1997) 1091.
[31] U. Hersel, C. Dahmen, H. Kessler, Biomaterials 24 (2003) 4385.
[32] E.G. Hayman, M.D. Pierschbacher, S. Suzuki, E. Ruoslahti, Exp. Cell Res. 160 (1985) 245.
[33] F. Grinnell, M.K. Feld, J. Biol. Chem. 257 (1982) 4888.
[34] H. Liang, H. Miranto, N. Granqvist, J.W. Sadowski, T. Viitala, B. Wang, M. Yliperttula, Sens. Actuator B-Chem. 149 (2010) 212.
[35] K.S. Kontturi, E. Kontturi, J. Laine, J. Mater. Chem. A 1 (2013) 13655.
[36] J.J. Valle-Delgado, L.S. Johansson, M. Österberg, Colloid Surf. B-Biointerfaces 138 (2016) 86.
[37] C.E. Jordan, B.L. Frey, S. Kornguth, R.M. Com, Langmuir 10 (1994) 3642.
[38] J. Vörös, Biophys. J. 87 (2004) 553.
[39] R.W.N. Nugroho, R. Harjumäki, X. Zhang, Y.R. Lou, M. Yliperttula, J.J. Valle-Delgado, M. Österberg, Colloid Surf. B-Biointerfaces 173 (2019) 571.
[40] P. Eronen, K. Junka, J. Laine, M. Österberg, BioResources 6 (2011) 4200.
[41] S. Ahola, J. Salmi, L.S. Johansson, J. Laine, M. Österberg, Biomacromolecules 9 (2008) 1273.
[42] J.E. Bottenstein, G.H. Sato, Proc. Natl. Acad. Sci. USA 76 (1979) 514.
[43] D.M. Bissell, D.M. Arenson, J.J. Maher, F.J. Roll, J. Clin. Invest. 79 (1987) 801.
[44] B.S. Jacobson, D. Branton, Science 195 (1977) 302.
[45] L. Richert, Y. Arntz, P. Schaaf, J.C. Voegel, C. Picart, Surf. Sci. 570 (2004) 13.
[46] C. Perrino, S. Lee, S.W. Choi, A. Maruyama, N.D. Spencer, Langmuir 24 (2008) 8850.
[47] S. Ahola, P. Myllytie, M. Österberg, T. Teerinen, J. Laine, BioResources 3 (2008) 1315.
[48] J. Hoja, R.J. Maurer, A.F. Sax, J. Phys. Chem. B 118 (2014) 9017.
[49] D.S. Zimnitsky, T.L. Yurkshtovich, P.M. Bychkovsky, J. Colloid Interface Sci. 285 (2005) 502.
[50] V.M. Sedelkin, T.O. Ryabukhova, N.A. Okisheva, M.G. Pozdeeva, Russ. J. Appl. Chem. 80 (2007) 58.
[51] J. Lucenius, K. Parikka, M. Österberg, React. Funct. Polym. 85 (2014) 167.
[52] J. Stiernstedt, N. Nordgren, L. Wågberg, H. Brumer, D.G. Gray, M.W. Rutland, J. Colloid Interface Sci. 303 (2006) 117.
[53] J.U. Park, T. Ishihara, A. Kano, T. Akaike, A. Maruyama, Prep. Biochem. Biotechnol. 29 (1999) 353.
[54] N. Kawakami-Kimura, T. Narita, K. Ohmori, T. Yoneda, K. Matsumoto, T. Nakamura, R. Kannagi, Br. J. Cancer 75 (1997) 47.
[55] J. Wakayama, H. Sekiguchi, S. Akanuma, T. Ohtani, S. Sugiyama, Anal. Biochem. 380 (2008) 51.
[56] X. Wang, X. Xing, B. Zhang, F. Liu, Y. Cheng, D. Shi, Int. J. Nanomed. 9 (2014) 1601.
[57] R. Harjumäki, X. Zhang, R.W.N. Nugroho, M. Farooq, Y.R. Lou, M. Yliperttula, J.J. Valle-Delgado, M. Österberg, ACS Appl. Bio Mater. 3 (2020) 1406.
[58] G. Gstraunthaler, Altex Altern. Tierexp. 20 (2003) 275.